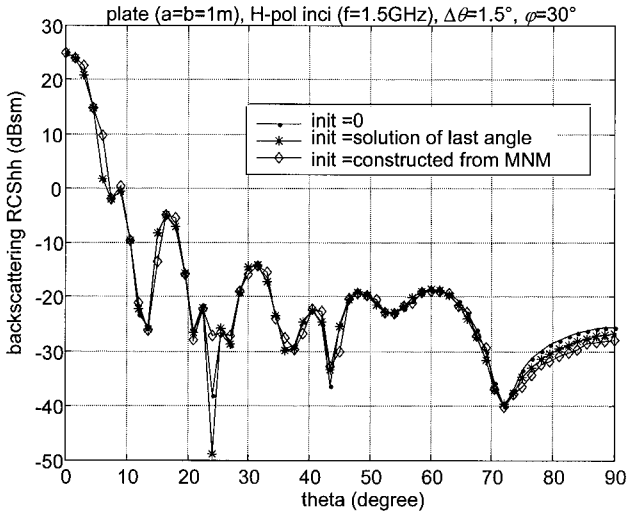

Figure 6 Comparison of backscattered RCS versus angle when different initial values are used for the plate scattering problem ($\phi = 30$, $\Delta\theta = 1.5$)

unexpectedly, increasing the angular increment $\Delta\theta$ exacerbates the problem. When angle step is set to 3°, more information of the backscattering RCS variation versus angle was missing for both $\phi = 0$ and 30° cuts. So the angle step should be less than 1.5° for this case.

In Table 1, CGNtol is the CGN stopping criteria, N and tol are the number of vectors and error tolerance used in the MNM process. The total time saving (Tsave) is calculated by using the following formula

$$T_{\text{save}} = (T_{\text{zero}} - T_{\text{MNM}})/T_{\text{zero}} \times 100\%, \quad (6)$$

where T_{zero}, T_{MNM} is the total CPU time when zero initial guess and MNM constructed initial guess is used in the computation, respectively.

4. CONCLUSION

The MNM technique, originally developed for frequency sweeping in the context of RCS computation, has been extended in this Letter to speed up the iterative solution of MoM matrix equations with multiple right–hand-sides, corresponding to different angles of incidence. It has been shown that the use of this technique can reduce the computation time without sacrificing the accuracy of the solution. The MNM itself places little additional computational burden on the iteration process, and it usually takes less than the time required for single iteration in the CG process. The time saving realized over the zero initial guess can be significant, especially when the angular increment is small, which is needed to capture the rapid variation of the RCS, typically associated with large or complex scatterers.

ACKNOWLEDGMENT

The authors gratefully acknowledge the help received from Dr. Larry Carin and his group at Duke University for providing the FMM code used in this research. The authors are also thankful to Professor Antoine Tijhuis, whose group has independently developed a similar technique, for helpful discussions.

REFERENCES

1. V.P. Abeele, L. Knockaert, and D.D. Zutter, Convergence analysis and operation count of the conjugate gradient fast multipole method, IEEE AP-S International Symposium, Atlanta, July 1998, Vol. 3, pp. 1750–1753.
2. V. Rokhlin, Rapid solution of integral equations of scattering theory in two dimension, J Comput Phys 86 (1990), 414–430.
3. N. Geng, A. Sullivan, and L. Carin, Multilevel fast-multipole algorithm for scattering from conducting targets above or embedded in a lossy half space, IEEE Trans Geosci Remote Sensing GRS-38 (2000), 1561–1573.
4. R. Mittra, V.V.S. Prakash, J.F. Ma, S.P. Benham, and J. Lord, MNM—A novel technique for the iterative solution of matrix equations arising in the method of moments formulation," CEM2002 symposium, Bath, U.K., April 2002.
5. R. Mittra, V.V.S. Prakash, J.F. Ma, J. Yeo, N. Huang, and S. J. Kwon, A novel technique for iterative solution of matrix equation arising in the method of moments formulation, Microwave Opt Technol Lett, in press.
6. J.F. Ma, R. Mittra, and N. Huang, Improving the convergence of the iterative solution of matrix equations in the method of moments formulation using extrapolation techniques, IEE Proc Pt H, in press.

© 2002 Wiley Periodicals, Inc.

CAD OF COAXIALLY END-FED WAVEGUIDE PHASED-ARRAY ANTENNAS

Vincenzo Galdi,[1,2] Giampiero Gerini,[3] Marco Guglielmi,[4] Huib J. Visser,[5] and Francesco D'Agostino[6]
[1] Department of Electrical and Computer Engineering
Boston University
8 Saint Mary's Street
Boston Massachusetts 02215
[2] Waves Group
University of Sannio
Piazza Roma, Palazzo Bosco Lucarelli
I-82100 Benevento, Italy
[3] TNO Physics and Electronics Laboratory
P.O. Box 96864
2509 JG The Hague, The Netherlands
[4] European Space Research and Technology Centre (ESTEC)
P.O. Box 299
2200 AG Noordwijk, The Netherlands
[5] TNO—Industrial Technology
P.O. Box 6235
5600 HE Eindhoven, The Netherlands
[6] D.I.I.I.E.
University of Salerno
Via Ponte Don Melillo
I-84084 Fisciano (SA), Italy

Received 18 February 2002

ABSTRACT: *An alternative configuration for an infinite coaxially end-fed waveguide phased-array antenna is explored. In the proposed configuration, the integration of the end-fed launcher and the output waveguide, rather than the waveguide in itself, acts as a basic radiator. This allows the design of more compact antenna elements. In order to analyze and optimize the structure, an accurate full-wave simulation tool based on the multimode admittance matrix representation is developed. Results are validated against state-of-the-art commercial CAD software. Numerical simulations involving singly and doubly tuned configurations are presented and discussed to illustrate the potential convenience of the proposed configuration and of the CAD tool developed.*
© 2002 Wiley Periodicals, Inc. Microwave Opt Technol Lett 34: 276–281, 2002; Published online in Wiley InterScience (www.interscience.wiley.com). DOI 10.1002/mop.10437

Contract grant sponsor: European Union; Contract grant number: ERBFMRXCT960050.

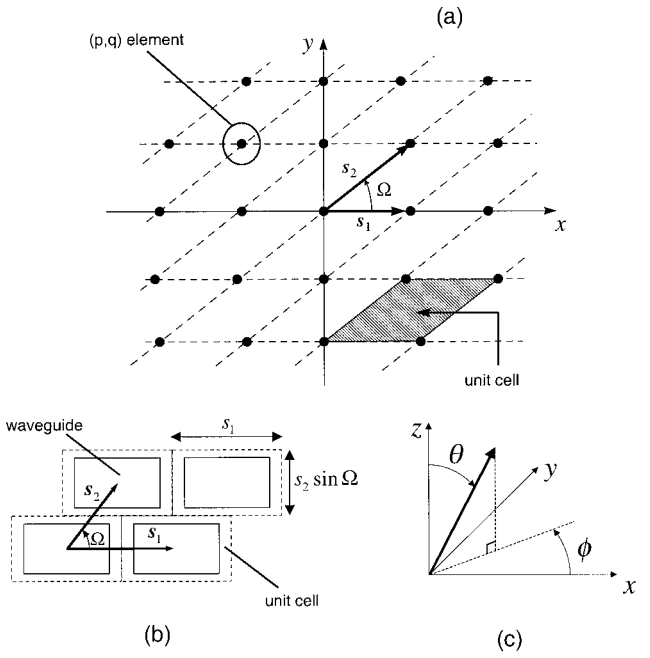

Figure 1 Problem geometry. (a): Infinite, regularly spaced array of radiators on a triangular lattice; (b) equivalent representation in terms of rectangular cells; (c) reference coordinate systems

Key words: *phased-array antennas; coaxial excitation; full-wave CAD tools*

1. INTRODUCTION

The current trend for waveguide phased arrays for space applications requires increased integration as well as strongly decreased development and manufacturing time and effort. As a consequence, new configurations need to be explored and more efficient CAD tools need to be developed. Toward this goal, a novel design approach, based on microwave filter concepts, was explored in [1]. This approach, valid for infinite periodic structures of identical waveguide radiators [Figure 1(a)], is based on the analysis of a single unit cell element, that is, basically, the transition from a metallic waveguide radiator to free space. Due to periodicity, the field in the free-space unit cell can be decomposed into Floquet modes, so that the cell is actually equivalent to a waveguide with phase-shift walls. The problem is thus reduced to a waveguide discontinuity problem similar to those typically encountered in microwave filter analysis. This suggests that the arsenal of CAD tools already available for microwave filter design can be used for phased-array design. Such an alternative design approach, in conjunction with a multimode equivalent network representation [2], has been applied successfully in [1], where it was validated against experimental data and found to provide significant additional degrees of freedom.

In this Letter the approach in [1] is applied to explore a waveguide phased-array configuration that uses as a basic radiator a coaxially end-fed waveguide launcher. In this configuration, the radiating element can be modeled as a conducting post, fed on the back by a coaxial excitation, radiating in free space through a short section of rectangular waveguide (see, for example, the unit cell in Figure 2). More specifically, this framework is based on the combined use of the full-wave CAD tool developed in [3] for rectangular waveguide filters with integrated coaxial transition and the design approach in [1].

Although the use of a coaxial-to-rectangular waveguide end launcher (possibly with a ridged sector) has been widely investigated in the technical literature (see, e.g., [4–8]), the novelty of the configuration proposed here lies in the fact that the end launcher is not only used for exciting the waveguide radiator, but is *itself* part of the radiator. Therefore, the rectangular waveguide does not need to be above cutoff over the useful bandwidth, and a more compact array can be obtained.

The remainder of the Letter is organized as follows. In Section 2, the problem geometry and its formulation are illustrated. In Section 3, the general multimode admittance representation is briefly reviewed and the structure of the CAD tool developed is outlined. In Section 4, simulation results concerning two application examples are presented, and design criteria for their optimization are provided. Brief conclusions are given in Section 5.

2. PROBLEM FORMULATION

An infinite, regularly spaced array of identical waveguide radiators arranged on a two-dimensional (2D) triangular lattice in the $x - y$ plane is considered, as shown in Figure 1(a). In this lattice, the position of the (p, q) element is given by

$$\mathbf{r}_{pq} = p\mathbf{s}_1 + q\mathbf{s}_2 \begin{cases} \mathbf{s}_1 = s_1\mathbf{u}_x, \\ \mathbf{s}_2 = s_2(\cos\Omega\mathbf{u}_x + \sin\Omega\mathbf{u}_y). \end{cases} \tag{1}$$

Here and henceforth, boldface symbols denote vector quantities, and $\mathbf{u}_\alpha$ denotes an α-directed unit vector. The structure in Figure 1(a) admits an equivalent representation in terms of rectangular cells [1], as shown in Figure 1(b). Due to periodicity, only the basic unit cell needs to be studied [9], and the transverse fields in the free-space unit cell can be expanded into Floquet modes as [1, 10]

$$\mathbf{E}_t(x, y, z) = \sum_{p,q=-\infty}^{\infty} V_{pq}(z)\mathbf{e}_{pq}(x, y),$$

$$\mathbf{H}_t(x, y, z) = \sum_{p,q=-\infty}^{\infty} I_{pq}(z)\mathbf{h}_{pq}(x, y), \tag{2}$$

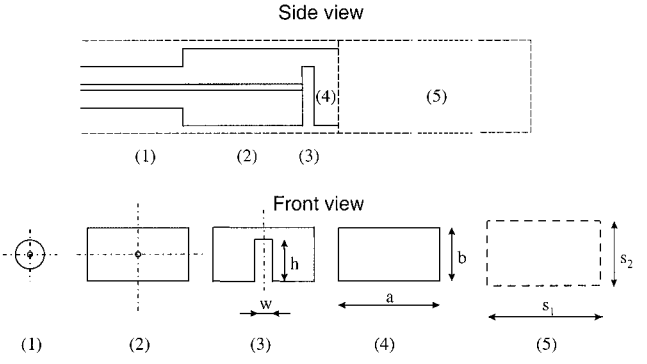

Figure 2 Singly-tuned configuration: array unit cell: (1) Coaxial cable (internal radius: 0.65 mm, external radius: 2.05 mm, relative dielectric permittivity: $\varepsilon_r = 2.08$, length: 5 mm). (2) Coaxial waveguide with rectangular cross section (internal radius: 0.65 mm, external sides: $a = 15.799$ mm, $b = 7.899$ mm, length: 6.3 mm). (3) Ridge waveguide (sides: $a = 15.799$ mm, $b = 7.899$ mm, ridge dimensions: $w = 1.62$ mm, $h = 5.8$ mm, length: 1.1 mm). (4) Rectangular waveguide ($a = 15.799$ mm, $b = 7.899$ mm, length: 2 mm). (5) Phase-shift waveguide ($s_1 = 16.8$ mm, $s_2 = 8.9$ mm, $\Omega = \pi/2$, length: 2400 mm)

where V_{pq} and I_{pq} are modal voltage and current, respectively, and a time-harmonic $\exp(j\omega t)$ dependence is assumed and omitted. The electric and magnetic Floquet vector mode functions $\mathbf{e}_{pq}$ and h_{pq}, respectively, are solutions of the Helmholtz equation with periodic boundary conditions at the walls of the cell, and admit the following expressions [1, 10]:

- TE modes

$$\begin{cases} \mathbf{e}_{pq}^{\mathrm{TE}}(x,y) = -\dfrac{1}{k_{tpq}\sqrt{s_1 s_2 \sin\Omega}} & \left\{ \begin{array}{l} (k_{ypq}\mathbf{u}_x - k_{xp}\mathbf{u}_y) \\ \quad \times \exp[-j(k_{xp}x + k_{ypq}y)], \end{array} \right\} \\ \mathbf{h}_{pq}^{\mathrm{TE}} = \mathbf{u}_z \times \mathbf{e}_{pq}^{\mathrm{TE}}, \end{cases} \tag{3}$$

- TM modes

$$\begin{cases} \mathbf{e}_{pq}^{\mathrm{TM}}(x,y) = -\dfrac{1}{k_{tpq}\sqrt{s_1 s_2 \sin\Omega}} & \left\{ \begin{array}{l} (k_{xp}\mathbf{u}_x + k_{ypq}\mathbf{u}_y) \\ \quad \times \exp[-j(k_{xp}x + k_{ypq}y)], \end{array} \right\} \\ \mathbf{h}_{pq}^{\mathrm{TM}} = \mathbf{u}_z \times \mathbf{e}_{pq}^{\mathrm{TM}}, \end{cases} \tag{4}$$

where $k_{tpq} = \sqrt{k_{xp}^2 + k_{ypq}^2}$ and

$$k_{xp} = k_0 \sin\theta\cos\phi + \frac{2\pi p}{s_1}, \qquad p = 0, \pm 1, \pm 2, \ldots, \tag{5}$$

$$k_{ypq} = k_0 \sin\theta\sin\phi - \frac{2\pi p}{s_1 \tan\Omega} + \frac{2\pi q}{s_2 \sin\Omega}, \qquad p, q = 0, \pm 1, \pm 2, \ldots. \tag{6}$$

In (5) and (6), $k_0 = \omega\sqrt{\varepsilon_0\mu_0}$ denotes the free-space wave number, and θ, ϕ are the spherical coordinate angles in Figure 1(c).

The basic structure of the waveguide phased-array unit cell is thus constituted by a cascade of a number of uniform waveguide sections (the radiator) and a phase-shift waveguide termination (free space). Looking, for instance, at the configuration in Figure 2, starting from the left, one first finds a length of dielectric loaded coaxial waveguide (the feeding connector), then a section of coaxial waveguide with rectangular cross section (CWRCS), a section of ridge waveguide (the radiating element), a section of rectangular waveguide (output coupling), and finally a phase-shift waveguide.

The electrical behavior of the complete unit cell can easily be analyzed in terms of a global admittance matrix representation [2].

3. MULTIMODE EQUIVALENT NETWORK REPRESENTATION OF THE BASIC UNIT CELL

Following the theory in [2], each step junction between the various waveguides in the array unit cell is described in terms of local admittance matrices, and the problem is reduced to the computation of the modes of each uniform waveguide region, and of the coupling integrals (standard inner products) between modes at each step junction (see [2] for details).

These computations do not pose any problem for the sections of circular-coaxial and rectangular waveguides [3], and therefore the relevant details are not discussed. The (Floquet) modes of the phase-shift waveguide are given in (3) and (4), and their coupling integrals with the standard rectangular waveguide modes are reported in the Appendix. The modal analysis of the CWRCS and of the ridge waveguide have been performed with the use of the boundary integral resonant mode expansion method detailed in [11]. This technique is indeed very accurate and efficient and, in addition, gives the coupling integrals between the ridge waveguide and the standard rectangular waveguide directly [12]. The computation of the coupling integrals between the ridge waveguide and the CWRCS requires a small additional effort, basically consisting of employing an intermediate step involving the coupling to a rectangular waveguide (see [3] for details).

Once all coupling integrals are available, the procedure described in [13] is used to evaluate efficiently the required admittance matrix parameters. The complete unit cell is thus represented in terms of a global equivalent circuit, from which the electrical behavior of the phased-array unit cell is finally obtained by solving an associated banded linear system [14]. The reader is referred to [1, 2] for computational details and convergence issues. Note that unlike standard mode-matching techniques, the proposed method is *uniformly* convergent [1, 2].

Most of the attractive computational features of the the multimode equivalent network representation utilized in this approach stem from its inherent *modularity*. This allows, in principle, straightforward analysis of structures such as, for example, dielectric radomes and frequency-selective surfaces *integrated* with the antenna. Such extensions have already been explored in [1] for planar arrays and in [15] for conformal cylindrical arrays, in conjunction with a new integral equation formulation [16]. Modularity is also a highly desirable feature in computer optimization design procedures. Using the present approach, in fact, only those parts of the complete structure that have actually been modified need to be characterized again, with the multimode network representation of the rest of the structure kept unchanged. Moreover, if the tuning is mainly achieved by acting on the longitudinal dimensions of the waveguide sections, there is no need to recompute the modes and the coupling integrals, which have been evaluated and properly stored in the previous iterations. Clever exploitation of the above features allows for substantial speedup in optimization procedures when many iterations are required to meet the design specifications.

4. RESULTS

The first structure considered is the infinite array of the basic elements shown in Figure 2 placed on a periodic rectangular lattice ($\Omega = \pi/2$). The structure has been designed to exhibit a resonance at about 10 GHz. In this connection, it was found that the resonant frequency can be easily controlled by varying the height of the post, whereas the bandwidth can be adjusted by changing the

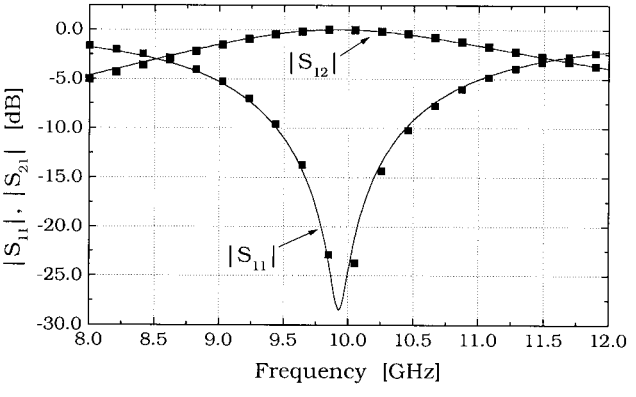

Figure 3 Singly-tuned configuration in Figure 2. Frequency response (scattering matrix parameters) of the array unit cell at broadside ($\theta = 0$) computed with the use of the proposed method is compared with Ansoft HFSS prediction. Solid lines, proposed method; squares, HFSS

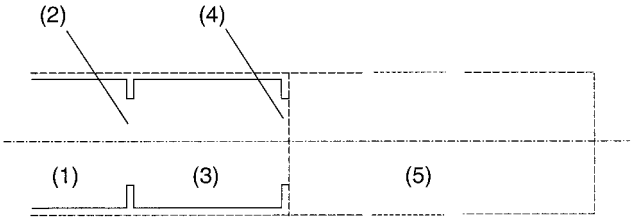

Figure 4 Singly tuned configuration using rectangular resonators: array unit cell (side view). (1) Rectangular waveguide (a = 19.05 mm, b = 9.525 mm, length: 10 mm). (2) Rectangular waveguide (a = 12 mm, b = 9 mm, length: 2 mm). (3) Rectangular waveguide (a = 19.05 mm, b = 9.525 mm, length: 16.50 mm). (4) Rectangular waveguide (a = 12 mm, b = 9 mm, length: 1 mm). (5) Phase-shift waveguide (s_1 = 20.05 mm, s_2 = 10.525 mm, $\Omega = \pi/2$, length: 2400 mm)

contact position of the coaxial feed on the radiating post or acting on the length of the CWRCS and on the length of the empty rectangular waveguide. The optimized frequency response of the array unit cell at broadside ($\theta = 0$) is shown in Figure 3 in terms of scattering matrix parameters, and is compared to the results obtained with the use of the commercial CAD software Ansoft HFSS-8.0.25 [17]. Good agreement is observed, confirming the accuracy of the proposed full-wave CAD tool. It is interesting to note that the electrical behavior of the array unit cell is identical to that of a one-resonator interdigital filter if one views the input coaxial connection and the rectangular waveguide as input and output coupling, respectively, and the ridge waveguide section as a lumped resonator.

In order to highlight the advantages of the configuration proposed in this article, an array composed of unit cells consisting of cascaded standard rectangular waveguides only is considered (Figure 4). Attempts were made to optimize the structure so as to achieve a frequency response close to that in Figure 3, while keeping the transverse dimensions of the unit cell not very different. One of the best syntheses obtained is shown in Figure 5; as one can see, the bandwidth achieved is smaller. In order to obtain a wider bandwidth, one should increase the dimensions of the feeding rectangular waveguides, thereby increasing the value of the array spatial periods s_1 and s_2. However, this would have the undesired effect of exciting higher-order Floquet harmonics (grating lobes) in the operating band. Looking at the radiation pattern, at a fixed frequency and azimuthal angle ϕ [see Figure 1(c)], there exists a critical elevation angle θ_c beyond which the higher-order

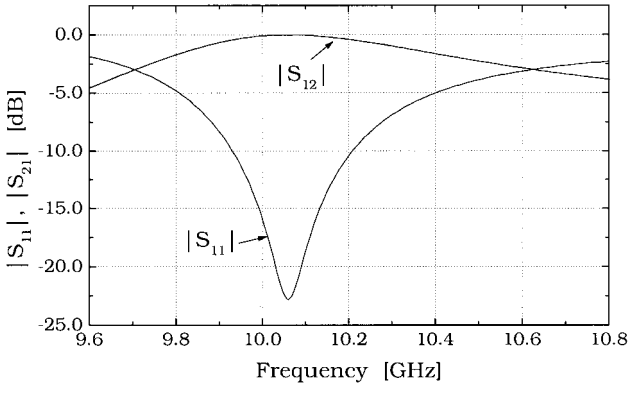

Figure 5 Singly tuned configuration with rectangular resonators in Figure 4. Frequency response (scattering matrix parameters) of the array unit cell at broadside ($\theta = 0$) computed with the use of the proposed method

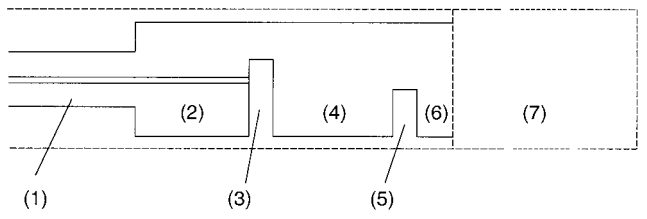

Figure 6 Doubly tuned configuration: array unit cell (side view). (1) Coaxial cable (internal radius: 0.65 mm, external radius: 2.05 mm, relative dielectric permittivity: ε_r = 2.08, length: 5 mm); (2) Coaxial waveguide with rectangular cross section (internal radius: 0.65 mm, external sides: a = 15.799 mm, b = 7.899 mm, length: 6.3 mm). (3) Ridge waveguide (sides: a = 15.799 mm, b = 7.899 mm, ridge dimensions: w = 1.62 mm, h = 5.8 mm, length: 1.1 mm). (4) Rectangular waveguide (a = 15.799 mm, b = 7.899 mm, length 9.2 mm). (5) Ridge waveguide (sides: a = 15.799 mm, b = 7.899 mm, ridge dimensions: w = 1.62 mm, h = 4.12 mm, length: 1.1 mm). (6) Rectangular waveguide (a = 15.799 mm, b = 7.899 mm, length 2.6 mm). (7) Phase-shift waveguide (s_1 = 16.8 mm, s_2 = 8.9 mm, $\Omega = \pi/2$, length: 2400 mm)

Floquet modes appear. For example, in the $x - z$ plane ($\phi = 0$) the critical angle θ_c (grating lobe condition) is defined by

$$\theta_c = \sin^{-1}\left(\frac{2\pi}{k_0 s_1} - 1\right). \tag{7}$$

At 10 GHz, for instance, the critical angle is about 29.8° for the standard rectangular waveguide array in Figure 3, against 51.8° obtained with the coaxially end-fed waveguide radiator in Figure 2. It is worth noting, however, that with the use of ridge radiators it is possible to further reduce the waveguide dimensions (and thus the spatial periods), thereby resulting in even wider ranges of single-mode radiation.

An unpleasant feature of the unit cell configuration in Figure 2 is that the power is not radiated uniformly over the useful bandwidth because the radiator is *singly tuned.* In this connection, the array performance can be improved by considering a *doubly tuned* unit cell, as in Figure 6. This structure has been obtained by adding another section of ridge waveguide between input and output. The structure has again been optimized for radiation at broadside. The frequency response of the array unit cell is shown in Figure 7, together with the HFSS prediction. As one can see, a typical equiripple two-pole Chebychev response has been obtained, so that

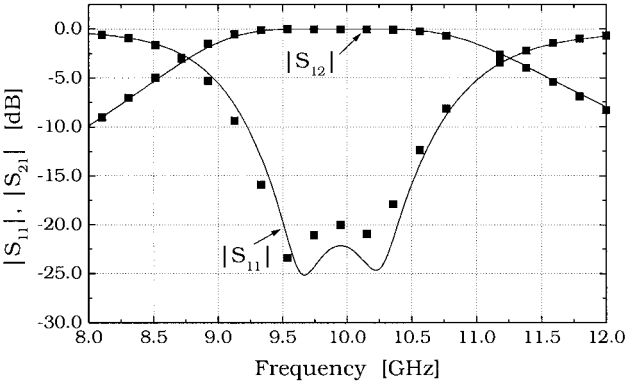

Figure 7 Doubly tuned configuration in Figure 6. Frequency response (scattering matrix parameters) of the array unit cell at broadside ($\theta = 0$) computed using the proposed method is compared with Ansoft HFSS prediction. Solid lines, proposed method; squares, HFSS

the structures now radiate almost uniformly over the complete useful bandwidth. Again, good agreement with the HFSS prediction is observed.

All simulations presented above have been performed on a PC Pentium II 350 MHz with 256MB RAM. The number of modes used in the various sections and other relevant simulation parameters were chosen according to the criteria provided in [1–3], resulting in typical overall computing times of a few minutes (for 50 frequency points), which are comparable with those of HFSS. However, as already stated in Section 3, the proposed approach turns out to be particularly suited for computer optimization design procedures in which the transverse dimensions of most waveguide sections are kept unchanged and the tuning is mainly achieved by acting on the longitudinal dimensions. In this case, in fact, a smarter implementation is possible, by storing the modes and the coupling integrals and thus avoiding their recomputation at each iteration, resulting in typical speedups of almost one order of magnitude.

5. CONCLUSIONS

An alternative configuration for waveguide phased arrays has been explored. Its basic element is essentially a coaxially end-fed waveguide launcher. An efficient full-wave CAD tool, based on a multimode admittance representation, has been developed. This CAD tool has been validated against a commercial full-wave CAD software, and has subsequently been used to analyze and optimize the structure.

Numerical results indicate that the proposed configuration is potentially attractive, as compared to standard rectangular waveguide phased arrays, in terms of compactness, bandwidth, and grating lobe performance.

APPENDIX—COUPLING INTEGRALS BETWEEN RECTANGULAR AND PHASE-SHIFT WAVEGUIDES

The coupling integrals regarding the junction between a rectangular waveguide and a phase-shift waveguide can be computed in closed form. For the simplest case, where the two waveguides are centered and nontilted, one finds

$$\langle \mathbf{h}_{pq}^{\mathrm{TM}}, \mathbf{h}_{nm}^{\mathrm{TM}} \rangle = \frac{2\left(k_{xp}\frac{n\pi}{a}F_2G_2 + k_{ypq}\frac{m\pi}{b}F_1G_1\right)}{k_{tpq}\sqrt{\left(\frac{n\pi}{a}\right)^2+\left(\frac{m\pi}{b}\right)^2}\sqrt{abs_1s_2\sin\Omega}}, \tag{8}$$

$$\langle \mathbf{h}_{pq}^{\mathrm{TM}}, \mathbf{h}_{nm}^{\mathrm{TE}} \rangle = -\frac{\varepsilon_{nm}\left(k_{xp}\frac{m\pi}{b}F_2G_2 - k_{ypq}\frac{n\pi}{a}F_1G_1\right)}{k_{tpq}\sqrt{\left(\frac{n\pi}{a}\right)^2+\left(\frac{m\pi}{b}\right)^2}\sqrt{abs_1s_2\sin\Omega}}, \tag{9}$$

$$\langle \mathbf{h}_{pq}^{\mathrm{TE}}, \mathbf{h}_{nm}^{\mathrm{TM}} \rangle = -\frac{2\left(k_{xp}\frac{m\pi}{b}F_1G_1 - k_{ypq}\frac{n\pi}{a}F_2G_2\right)}{k_{tpq}\sqrt{\left(\frac{n\pi}{a}\right)^2+\left(\frac{m\pi}{b}\right)^2}\sqrt{abs_1s_2\sin\Omega}}, \tag{10}$$

$$\langle \mathbf{h}_{pq}^{\mathrm{TE}}, \mathbf{h}_{nm}^{\mathrm{TE}} \rangle = -\frac{\varepsilon_{nm}\left(k_{xp}\frac{n\pi}{a}F_1G_1 + k_{ypq}\frac{m\pi}{b}F_2G_2\right)}{k_{tpq}\sqrt{\left(\frac{n\pi}{a}\right)^2+\left(\frac{m\pi}{b}\right)^2}\sqrt{abs_1s_2\sin\Omega}}, \tag{11}$$

$$\varepsilon_{nm} = \sqrt{\varepsilon_n\varepsilon_m}, \qquad \varepsilon_v = \begin{cases} 1, & \text{if } v = 0, \\ 2, & \text{if } v \neq 0. \end{cases} \tag{12}$$

In (8)–(12), the indices (p, q) refer to the Floquet modes in the phase-shift waveguide, whereas (n, m) refer to the modes in the rectangular waveguide [18]. Moreover, k_{xp} and k_{ypq} are defined in (4) and (5), a and b denote the transverse dimensions of the rectangular waveguide, and

$$F_1 = \begin{cases} b, & \text{if } \dfrac{m\pi}{b} = k_{ypq} = 0, \\ \dfrac{b}{2}\exp\left(j\dfrac{m\pi}{2}\right), & \text{if } \dfrac{m\pi}{b} = k_{ypq} \neq 0, \\ -j\dfrac{k_{ypq}}{\left(\frac{m\pi}{b}\right)^2 - k_{ypq}^2}\left[(-1)^m\exp\left(-jk_{ypq}\dfrac{b}{2}\right) - \exp\left(jk_{ypq}\dfrac{b}{2}\right)\right], & \text{if } \dfrac{m\pi}{b} \neq k_{ypq}, \end{cases} \tag{13}$$

$$F_2 = \begin{cases} a, & \text{if } \dfrac{n\pi}{a} = k_{xp} = 0, \\ \dfrac{a}{2}\exp\left(j\dfrac{n\pi}{2}\right), & \text{if } \dfrac{n\pi}{a} = k_{xp} \neq 0, \\ -j\dfrac{k_{xp}}{\left(\frac{n\pi}{a}\right)^2 - k_{xp}^2}\left[(-1)^n\exp\left(-jk_{xp}\dfrac{a}{2}\right) - \exp\left(jk_{xp}\dfrac{a}{2}\right)\right], & \text{if } \dfrac{n\pi}{a} \neq k_{xp}, \end{cases} \tag{14}$$

$$G_1 = \begin{cases} 0, & \text{if } \dfrac{n\pi}{a} = k_{xp} = 0, \\ -j\dfrac{a}{2}\exp\left(j\dfrac{n\pi}{2}\right), & \text{if } \dfrac{n\pi}{a} = k_{xp} \neq 0, \\ -\dfrac{(n\pi/a)}{\left(\dfrac{n\pi}{a}\right)^2 - k_{xp}^2}\left[(-1)^n \exp\left(-jk_{xp}\dfrac{a}{2}\right) - \exp\left(jk_{xp}\dfrac{a}{2}\right)\right], & \text{if } \dfrac{n\pi}{a} \neq k_{xp}, \end{cases} \tag{15}$$

$$G_2 = \begin{cases} 0, & \text{if } \dfrac{m\pi}{b} = k_{ypq} = 0, \\ -j\dfrac{b}{2}\exp\left(j\dfrac{m\pi}{2}\right), & \text{if } \dfrac{m\pi}{b} = k_{ypq} \neq 0, \\ -\dfrac{(m\pi/b)}{\left(\dfrac{m\pi}{b}\right)^2 - k_{ypq}^2}\left[(-1)^m \exp\left(-jk_{ypq}\dfrac{b}{2}\right) - \exp\left(jk_{ypq}\dfrac{b}{2}\right)\right], & \text{if } \dfrac{m\pi}{b} \neq k_{ypq}. \end{cases} \tag{16}$$

The coupling integrals involving transverse electric fields are readily obtained from the above expressions as

$$\langle \mathbf{e}_{pq}, \mathbf{e}_{nm} \rangle = (-1)^{n+m+1} \langle \mathbf{h}_{pq}, \mathbf{h}_{nm} \rangle^*, \tag{17}$$

where the asterisk denotes complex conjugation.

REFERENCES

1. H.J. Visser and M. Guglielmi, CAD of waveguide array antennas based on "filter" concepts, IEEE Trans Antennas Propagat AP-47 (1999), 542–548.
2. A.A. Melcon, G. Connor, and M. Guglielmi, New simple procedure for the computation of the multimode admittance or impedance matrix of planar waveguide junctions, IEEE Trans Microwave Theory Tech MTT-44 (1996), 413–418.
3. G. Gerini and M. Guglielmi, Full-wave CAD of a rectangular waveguide filter with integrated coaxial transition, IEEE Trans Microwave Theory Tech MTT-49 (2001), 986–989.
4. G.J. Wheeler, Broadband waveguide-to-coaxial transitions. In IRE National Convention Record, 1957, Vol. 5, Part 1, pp. 182–185.
5. R. Tang and N.S. Wong, Multimode phased array element for wide scan angle impedance matching, Proc IEEE 56 (1968), 1951–1959.
6. B.N. Das and G.S. Sanyal, Coaxial-to-waveguide transition (end-launcher type), Proc IEE 123 (1976), 984–986.
7. A. Tadachi and M. Sato, Waveguide to coaxial converter, U.S. Patent 4,652,839, March 24, 1987.
8. S.M. Saad, A more accurate analysis and design of coaxial-to-rectangular waveguide end launcher, IEEE Trans Microwave Theory Tech MTT-38 (1990), 129–134.
9. C.A. Balanis, Antenna theory, John Wiley & Sons, New York, 1996.
10. I. Palócz and A.A. Oliner, Equivalent network of a multimode grating, IEEE Trans Microwave Theory Tech MTT-18 (1970), 244–252.
11. G. Conciauro, M. Bressan, and C. Zuffada, Waveguide modes via an integral equation leading to a linear matrix eigenvalue problem, IEEE Trans Microwave Theory Tech MTT-32 (1984), 1495–1504.
12. P. Arcioni, Fast evaluation of modal coupling coefficients of waveguide step discontinuities, IEEE Microwave Guided Wave Lett GWL-6 (1996), 232–234.
13. V.E. Boria and M. Guglielmi, Accelerated computation of admittance parameters for planar waveguide junctions, Int J Microwave Millimiter Wave Computer-Aided Eng, Vol. 7 (1997), 195–205.
14. V.E. Boria, G. Gerini, and M. Guglielmi, Efficient inversion technique for banded linear systems, Proc 1997 IEEE-MTT Int. Symp., Denver, 1997, Vol. 3, pp. 1567–1570.
15. G. Gerini and L. Zappelli, CAD of multilayer conformal cylindrical arrays, Proc. 2001 IEEE Antennas Propagat. Society Int. Symp., Boston, 2001, Vol. 3, pp. 816–819.
16. G. Gerini, M. Guglielmi, and G. Lastoria, Efficient integral equation formulations for admittance or impedance representations of planar waveguide junctions, Proc. 1998 IEEE MTT Int. Symp., Baltimore, 1998, Vol. 3, pp. 1747–1750.
17. Ansoft Corporation, ANSOFT HFSS-8.0.25 User Guide Manual.
18. N. Marcuvitz, Waveguide handbook, McGraw-Hill, New York, 1951.

© 2002 Wiley Periodicals, Inc.

WATER QUALITY STUDIES OF COMBINED OPTICAL, THERMAL INFRARED, AND MICROWAVE REMOTE SENSING

Yuanzhi Zhang, Jouni Pulliainen, Sampsa Koponen, and Martti Hallikainen
Department of Electrical and Communications Engineering
Laboratory of Space Technology
Helsinki University of Technology
Espoo 02150, Finland

Received 20 February 2002

ABSTRACT: *Two major water quality parameters can be estimated from optical, thermal infrared (IR), and microwave remotely sensed data. The results show that these data combined can result in better estimated accuracy than the optical retrieval of water quality observations. However, the technique still needs to be refined in future studies.* © 2002 Wiley Periodicals, Inc. Microwave Opt Technol Lett 34: 281–285, 2002; Published online in Wiley InterScience (www.interscience.wiley.com). DOI 10.1002/mop.10438

Key words: *water quality; remote sensing; regression analysis; neural network*

1. INTRODUCTION

Chlorophyll-a and turbidity are two major parameters affecting surface water quality, producing visible changes in the water surface [1]. Such changes in the spectral signals from the water surface should be measurable with satellite optical sensors [2, 3], but chlorophyll-a was mapped in the 1970s [4]. Up until now, the digital evaluation of remotely sensed data at visible and near-infrared (IR) wavelengths has been used to estimate major water quality parameters. Present and near-future satellite sensors such